New Journal of Physics
The open–access journal for physics

Spatially highly resolved study of AFM scanning tip–quantum dot local interaction

S Kičin[1], A Pioda[1], T Ihn[1], M Sigrist[1], A Fuhrer[1], K Ensslin[1], M Reinwald[2] and W Wegscheider[2]

[1] Solid State Physics, ETH Zürich, 8093 Zürich, Switzerland
[2] Institut für experimentelle und angewandte Physik, Universität Regensburg, Germany
E-mail: ensslin@phys.ethz.ch

New Journal of Physics **7** (2005) 185
Received 19 April 2005
Published 26 August 2005
Online at http://www.njp.org/
doi:10.1088/1367-2630/7/1/185

Abstract. Scanning-gate imaging of semiconductor quantum dots (QDs) promises access to probability distributions of quantum states. It could therefore be a novel tool for designing and optimizing tailored quantum states in such systems. A detailed study of a lithographically defined semiconductor QD in the Coulomb-blockade regime is presented, making use of the scanning-gate technique at a base temperature of 300 mK. The method allows a one-by-one manipulation of electrons in the structure. The obtained images interpreted with a suitable QD model guide the way to a local investigation of the electronic interior of the QD. Future perspectives of scanning-gate experiments on QDs are discussed.

PII: S1367-2630(05)98563-7

Contents

1. Introduction

The physical realization of quantum communication and quantum computing requires very precise control over the quantum states used to represent the elementary carrier of information, the qubit, and over the phase-coherent interaction between qubits [1, 2]. In the last 15 years, experimental physicists have made enormous progress in quantum dot (QD) fabrication and they have achieved impressive control over the dot's electronic charge [3, 4] and the properties of its individual orbital [5] and spin states [6]–[9]. As a consequence, proposals have been developed to utilize either orbital- or spin-degrees of freedom in QDs as the physical implementation of a qubit [10, 11]. Since then, QD design has been readily improved for achieving laterally defined QDs with one or two electrons [12] which exhibit the physics of (QD) hydrogen with only a single occupied state [12]–[14], or helium with its singlet ground state and its triplet excited state [12, 13, 15].

Parallel to these developments, scanning probe microscopy (SPM) techniques have been applied for the investigation of semiconductor nanostructures. Spatially resolved single-charge detection has, for example, been achieved using a scanning metallic single-electron transistor [16, 17]. Scanning experiments with only a sharp metallic tip coupled capacitively to a two-dimensional electron gas (2DEG) subject to a high magnetic field were interpreted in terms of the formation of a few-electron bubble forming underneath the tip [18]. SPM was also used to image coherent electron flow in the vicinity of a quantum point contact [19]. Similar experiments on quantum point contacts and quantum billiards were interpreted as showing the spatially resolved probability density distribution of quantum states [20].

Scanning-probe techniques can also be applied to QDs with the aim of extracting information about quantum states beyond that obtainable by transport experiments alone. These techniques potentially offer spatially resolved access to the properties of QDs. The enormous variety of methods that have been developed or are within reach, promise unforeseen further potential

for improving qubit design, preparation, interaction and measurement. Pioneering scanning experiments on QDs were reported by McEuen *et al* using dots forming at imperfections in carbon nanotubes [21]. They employed the so-called scanning-gate technique, in which a sharp scanning metallic tip couples capacitively to the QD under investigation. A lithographically fabricated semiconductor QD was recently studied with the same technique in [22, 23]. This type of experiment was theoretically investigated in [24]. Despite the experimental achievements, no experiment has so far presented convincing evidence for mapping QD wave functions or probability densities in real space and this issue remains one of the most challenging and important milestones for the extensive use of SPM for even more sophisticated experiments on single and coupled QD qubits.

In this paper, we present a detailed study of a lithographically defined semiconductor QD in the Coulomb blockade (CB) regime using the scanning-gate technique at a temperature of 300 mK. Compared with previous experiments, conductance resonances could be observed with the tip scanning at a constant height above the interior of the QD. The experimental results are discussed in terms of a QD model that captures the essential physics of the measurement. The tip–dot interaction potential was reconstructed from experimental data. Future perspectives of utilizing the scanning-gate technique for the investigation of QDs are discussed.

2. Sample, setup and description of the experiment

2.1. Sample fabrication and characterization

The QD under investigation was realized on a GaAs/AlGaAs heterostructure grown by molecular beam epitaxy containing a 2DEG with electron density of $5 \times 10^{11}\,\mathrm{cm}^{-2}$ and 34 nm below the surface. The electron mobility was determined to be $450\,000\,\mathrm{cm}^2\,\mathrm{V}\,\mathrm{s}^{-1}$ at a temperature of 4.2 K. In the first processing step, a $25 \times 25\,\mu\mathrm{m}^2$ mesa was defined by optical lithography and subsequent wet chemical etching. In the second step, many nanostructures were defined on the surface of the mesa by local anodic oxidation along certain lines using a room temperature scanning force microscope (SFM) [25]–[27]. The 2DEG is depleted below the oxide lines such that mutually isolated structures were realized (see figure 1(a)). Among them was the QD of interest here with a topographic size of $350 \times 400\,\mathrm{nm}^2$. The three quantum point contacts in the vicinity of the dot will not be further discussed in this paper.

Gates labelled 'G1' and 'G2' were used to tune the QD's coupling to source and drain reservoirs. The lateral plunger gate (PG) allowed to control the number of electrons in the dot. Figure 1(b) shows a measurement of the dot conductance as a function of the voltage U_{PG} on the PG. This measurement was taken at a temperature of 300 mK operating the QD in the CB regime. The average charging energy of the QD was determined from CB diamonds to be $\sim$0.8 meV. The average separation of single-particle energies estimated from the geometry of the QD is $\sim 30\,\mu$eV assuming a depletion length of 100 nm. The conductance resonances in figure 1(b) are thermally broadened with an electron temperature of 550 mK. Since the average single-particle level spacing is smaller than the thermal broadening of conductance resonances, we operate the dot in a few-level transport regime.

2.2. Preparation and description of the scanning-gate experiment

Scanning-gate measurements were performed using a home-built low temperature SFM operated in a He^3 cryostat with a base temperature of 300 mK [28]. A piezoelectric tuning fork sensor with

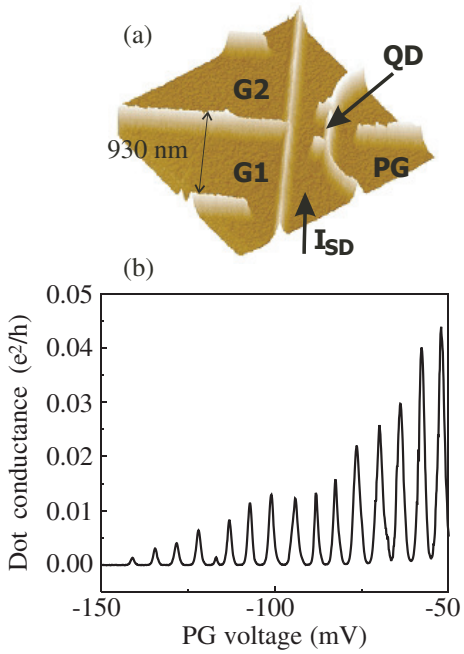

Figure 1. (a) Topography of the structure obtained by SFM at room temperature. Note that the microscope and tip used for acquiring this image differ from the cryogenic SFM equipment employed for the measurements presented in the following figures. (b) Conductance resonances measured by sweeping U_{PG} with $U_{SD} = 20\,\mu V$ symmetrically applied.

an electrochemically sharpened PtIr tip which could be electrostatically biased, was employed as the scanning probe [28].

Experiments similar to those presented below were performed before on another sample and on the sample presented here. Although scanning-gate images had been obtained in the CB regime, a direct study of the dot interior had not been possible due to a strong conductance increase when the negatively biased tip was positioned above the dot [22].

It turned out that in the experiments presented here, this conductance increase was not observed. Our present experience suggests that this may be due to the fact that, in contrast to previous cooldowns, we performed only scans at constant height above the surface (typically 60–150 nm) at base temperature. Before these scans, the QD was positioned in the centre of the scan range using the built-in coarse positioning x–y-motor and a series of topography scans on the surface with zero applied tip-voltage at an elevated temperature of 35 K. The aim of this procedure was to avoid any charging of the surface or charge rearrangements in the doping plane above the structure. The tip position with respect to the dot and the sharpness of the tip were again verified at the end of all experiments.

While the tip was scanned, the source–drain current I_{SD} was recorded. To this end, a low-frequency source–drain voltage $U_{SD} = 20\,\mu V$ was applied symmetrically (i.e., $+10\,\mu V$ applied to the source contact and $-10\,\mu V$ to the drain). The resulting ac I_{SD} was measured with a lock-in. Scanning-gate images, such as those presented in figure 2, are colour coded maps of the linear response dot conductance $G = I_{SD}/U_{SD} = dI_{SD}/dU_{SD}$ in the two-dimensional plane

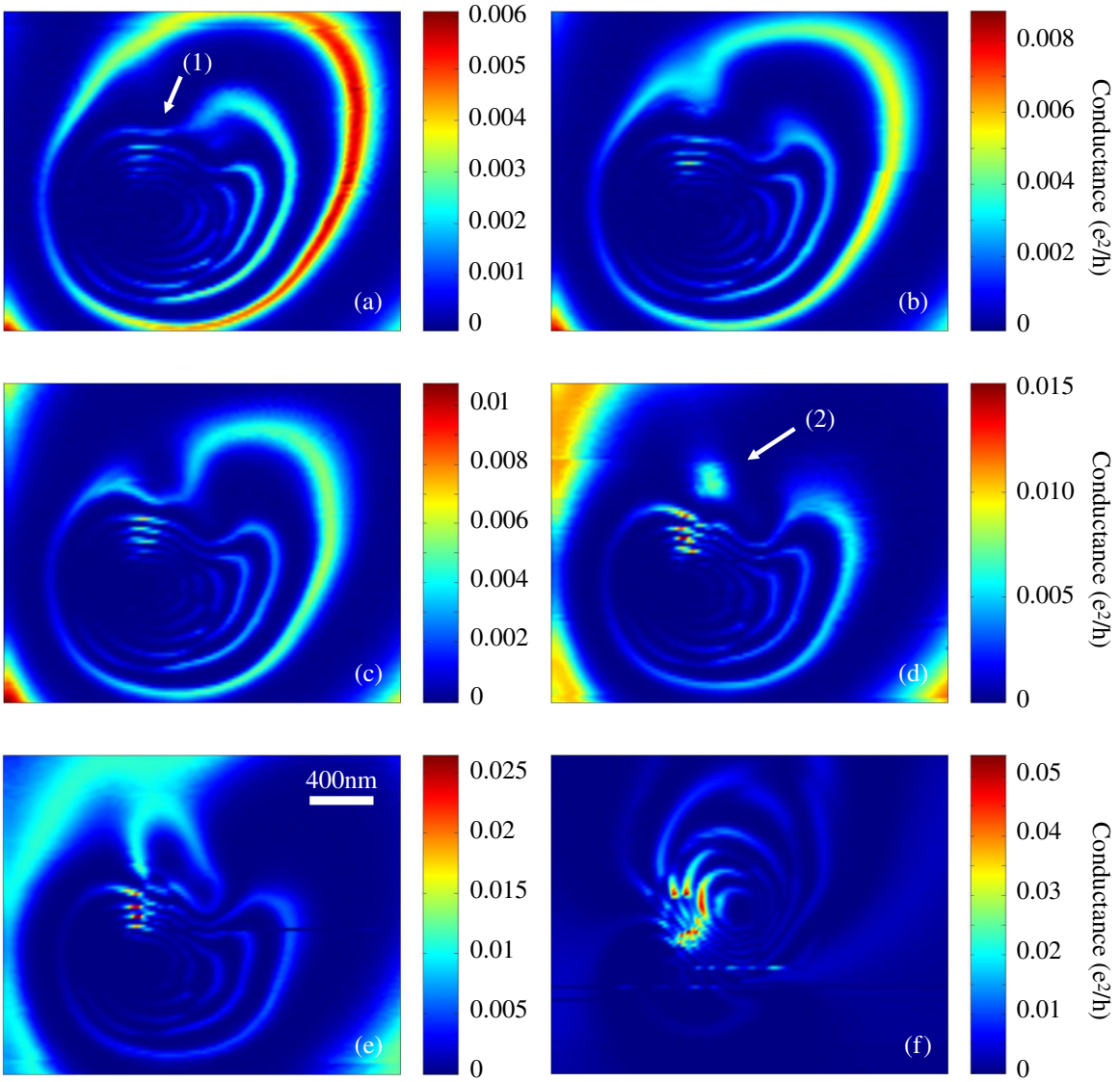

Figure 2. Scanning-gate images ($2500 \times 2000\,\mathrm{nm}^2$) obtained by varying U_{tip}. Tip-voltages are (a) $U_{\mathrm{tip}} = 0\,\mathrm{mV}$, (b) 30 mV, (c) 60 mV, (d) 120 mV, (e) 150 mV and (f) 510 mV.

of the tip position. The maximum resolution of the images was 88 000 pixel $\mu\mathrm{m}^2$ corresponding to a pixel separation of 3.37 nm.

Excellent reproducibility of the scans was found by repeating scans or by coming back to previous parameters after several other scans. During the experiment reported here, more than 300 scans were taken. During this time three significant changes of the QD state occurred making it necessary to readjust the gate voltages. At least two of these events corresponded to the appearance of a particle on the surface in the vicinity of the dot. These particles were detected in images of the tuning fork sensor frequency shift during constant height scans and verified by surface scanning at the end of the experiment. Each series of scanning-gate images presented below was recorded with the dot remaining in one of its stable states and during a single condensation cycle of the ^{3}He system.

3. Scanning-gate measurements

3.1. Tip-voltage dependence

Figure 2 shows scanning-gate images selected from a series taken at different tip-voltages between $U_{\mathrm{tip}} = 0$ (figure 2(a)) and 540 mV in steps of 15 mV. The tip was scanned at a distance of 150 nm from the surface. The images in figures 2(a)–(c) show a set of ring-shaped conductance resonances called 'set B' ('B' stands for 'bottom') around the location of the QD. Between the resonances, the current is blocked and the number of electrons in the dot is fixed to an integer value. Crossing a conductance resonance corresponds to changing the electron number in the dot by one.

The conductance rings show deformations of their shape, e.g., the one marked (1) in figure 2(a). In figure 2(d), a new conductance resonance spot marked (2) appears in the same location. For further increasing tip-voltages (figures 2(d)–(f)) another set of rings appears ('set T', where 'T' stands for 'top') around the position of the spot. The separation of the centres of the two sets 'B' and 'T' is more than 600 nm.

Closer inspection of 'set B' in figures 2(a)–(e) shows that the diameter of conductance resonance rings decreases continuously as a result of the increasing voltage. The image shown in figure 2(f) taken with $U_{\mathrm{tip}} = 510$ mV shows the situation where 'set T' dominates and 'set B' consists of only two fringes. For even higher tip-voltage (not shown), 'set B' completely disappears. In contrast to 'set B', the rings in 'set T' increase their diameter with increasing tip-voltage. In the following, we will show that the appearance of these two sets of fringes indicate the existence of a double-tip shape.

3.2. Model for the tip–dot interaction

We present a pragmatic model for the influence of the tip on the dot which is essentially based on the constant interaction model for QDs [29] taking the tip as an additional gate electrode with variable position into account. Although our experiments have not been performed in the single-level transport regime, we neglect transport through several levels in order to achieve a transparent and compact notation which still represents the underlying physics. With these simplifications, the energy required for adding an electron to the QD containing already $n-1$ excess electrons, i.e., the electrochemical potential μ_n, can be written as

$$\mu_n = \mu_n(\vec{r}; U_{tip}) = \varepsilon_n(\vec{r}; U_{tip}) - e\sum_i \alpha_i(\vec{r})\Delta U_i + n\frac{e^2}{C_\Sigma(\vec{r})}, \tag{1}$$

where $\vec{r}$ is the position of the tip. The last term on the right-hand side is the familiar charging energy term with the self-capacitance C_Σ leading—in the absence of the other two terms—to a ladder of equally spaced 'energy levels' in the dot for the number n of electrons running through a sequence of integer numbers. In the language of the Hartree approximation, e^2/C_Σ corresponds to the average Hartree energy per electron. The second term describes the influence of voltage changes ΔU_i on gate i which allow to shift the ladder of energy levels up or down according to the gate-dependent lever arm α_i. Within the Hartree approximation, each lever arm is the expectation value of the characteristic electrostatic function of the corresponding gate electrode evaluated with the relevant single-particle wave function in the QD. The last two terms taken together describe the contribution of the electrostatic potential to the electrochemical potential.

The first term in equation (1) is the contribution of the quantization of quantum states due to the confinement which can be seen as a single-particle energy level for the electron to be added in the bare confinement potential, or as the chemical potential for adding electron number n.

The action of the tip on the QD enters in equation (1) in several places. Firstly, the tip is one of the gate electrodes i that have a certain lever arm on the QD. It is obvious that the lever arm of the tip, α_{tip}, will depend on the position of the tip relative to the dot. If the tip–dot separation becomes much larger than the separation of other gates from the dot, α_{tip} will be very small compared to all other lever arms. Because all the α_i sum up to one due to fundamental arguments, the tip-position-dependence of α_{tip} will in general also imply the tip-position-dependence of all other lever arms. This effect can be interpreted as a result of screening, i.e., the metallic tip screens the electric field lines originating from a specific gate and ending on the QD. While the screening effect itself is (in our pragmatic approximation) independent of the voltages applied to gates and tip, the total second term in equation (1) depends linearly on the tip-voltage. This linear dependence can be seen as a result of a Taylor series expansion for small voltage changes around an operating point.

The second place where the presence of the tip enters equation (1) is the self-capacitance C_Σ of the QD. This quantity is the sum of all capacitance coefficients between gates and QD. When the position of the tip relative to the dot is changed, the mutual capacitance between the two is also changed implying a change in C_Σ. This effect can also be seen as the screening influence of the tip, because its presence allows to screen an additional charge on the dot in a spatial region, where no screening would occur in the absence of the tip. This screening effect is in our model independent of the tip-voltage (again, assuming small tip-voltage changes).

The third way how the tip enters equation (1) is by changing the single-particle wave function of the electron to be added and thereby the single-particle energy ε_n. For a weak tip-induced potential in the dot this effect may be treated by perturbation theory.

At this point, it is due to define what we call the interaction potential between the tip and the QD. When the tip is far away from the dot, its influence on the electrochemical potentials will be negligible and they will take on constant values $\mu_n^{(0)}$ independent of the exact tip position. In the following, we will call the tip-induced change $\Delta\mu_n(\vec{r}) = \mu_n(\vec{r}) - \mu_n^{(0)}$ the 'interaction potential between tip and dot'.

With this model of the electrochemical potential for adding an electron to the QD, we can express the (linear response) conductance through the dot in the weak-coupling regime as

$$G(\vec{r}) = \sum_n \frac{G_{\max}(\vec{r})}{\cosh^2\{[\mu_n(\vec{r}) - \mu_{SD}]/2kT\}}, \tag{2}$$

with

$$G_{\max}(\vec{r}) = \frac{e^2}{4kTh} \frac{\Gamma_L^{(n)}(\vec{r})\Gamma_R^{(n)}(\vec{r})}{\Gamma_L^{(n)}(\vec{r}) + \Gamma_R^{(n)}(\vec{r})}.$$

Here μ_{SD} is the electrochemical potential in the source and drain contacts, T is the electron temperature and $\Gamma_L^{(n)}$ and $\Gamma_R^{(n)}$ are the tunnel coupling constants of the nth level to the left (source) and right (drain) leads, respectively. The conductance shows thermally broadened resonances whenever one of the μ_n is equal to μ_{SD}. The conductance is exponentially suppressed, if μ_n differs by more than $2\,kT$ from resonance, implying that co-tunnelling is neglected in our model. In addition to the influence of the tip on μ_n discussed above, the tip also acts directly on the tunnel

coupling constants $\Gamma_L^{(n)}$ and $\Gamma_R^{(n)}$ making $G_{\max}$ tip-position-dependent as well. This modulates the amplitude of conductance resonances as a function of tip position.

3.3. Discussion of the data in the light of the model

The tip acts as a gate on the dot. In general, the gate voltages that tune the dot into the CB regime with the tip far away from the dot are not suitable for scanning-gate experiments with the tip close to the dot due to the screening effects mentioned above. In order to obtain a reasonable number of conductance resonances in a scanning-gate image, the tip-voltage U_{tip} and the PG voltage U_{PG} were optimized.

Following equation (2), the ring-shaped conductance resonances observed in figure 2 can be interpreted as lines of constant μ_n, i.e., as lines of constant interaction potential between the tip and the dot. The rings formed by conductance resonances correspond to a contour plot of the tip–dot interaction potential. The gradient of the interaction potential is directed normal to the contour lines of constant interaction. It is, however, not clear *a priori* in which direction the gradient vector points, i.e., in which direction the electron number in the dot decreases.

The answer to this question is given by the evolution of the rings in figure 2 with tip bias. With increasing tip-voltage the rings forming 'set B' contract. This means that the tip–dot interaction leading to 'set B' must be repulsive implying that the electron number in the dot decreases one by one as the tip is moved towards the central point of 'set B'. The appearance of a second 'set T' in which the rings expand with increasing tip bias is the evidence for an attractive interaction potential with its centre displaced by more than 600 nm from that of 'set B'. The total tip–dot interaction potential is a superposition of these two contributions.

These observations can be attributed to the existence of a double tip where each of the two tips must have its own contact potential difference. The repulsive tip–dot interaction for 'set B' and its disappearance beyond figure 2(f) suggests that the corresponding tip has a contact potential difference of about 0.55 V in agreement with earlier findings for PtIr tips on Ga[Al]As heterostructures [22, 30]. In contrast, the attractive tip–dot interaction potential for 'set T' and the disappearance of this set around 0 V suggests that the corresponding twin-tip has a contact potential difference close to 0 V. The material of this twin-tip must therefore be different from PtIr and it may be a semiconducting particle the tip has picked up during scans on the surface.

In fact, the tip-induced potential can be approximately reconstructed from the scanning-gate images in figure 2. We illustrate this in figure 3 using the data in figures 2(a) and (f). Firstly, the contour lines $\Delta\mu_n(\vec{r}_{tip} - \vec{r}_{dot}) = \text{const}$ are determined from the individual ring-shaped conductance resonance positions for which $\vec{r}_{dot}$ is fixed while $\vec{r}_{tip}$ is varying. In contrast, in a map of the tip-induced potential, the tip position would be fixed while $\vec{r}_{dot}$ would vary. Inversion of the space co-ordinates in $\Delta\mu_n(\vec{r}_{tip} - \vec{r}_{dot}) = \text{const}$ therefore gives the contour plots of the tip-induced potential as shown in figures 3(a) and (b) corresponding to the data in figures 2(a) and (f), respectively. Secondly, the average charging energy calculated from CB diamonds was assumed to dominate the energetic separation of neighbouring contour lines. This assumption allows one to convert the contour plot into the three-dimensional shapes of $\Delta\mu_n$ as shown in figures 3(c) and (d). The reconstructed shape is truncated because the dot was pinched off completely in the centre of the fringes. Figure 3(d) shows the double-tip structure with its positive and negative contribution to $\Delta\mu_n$.

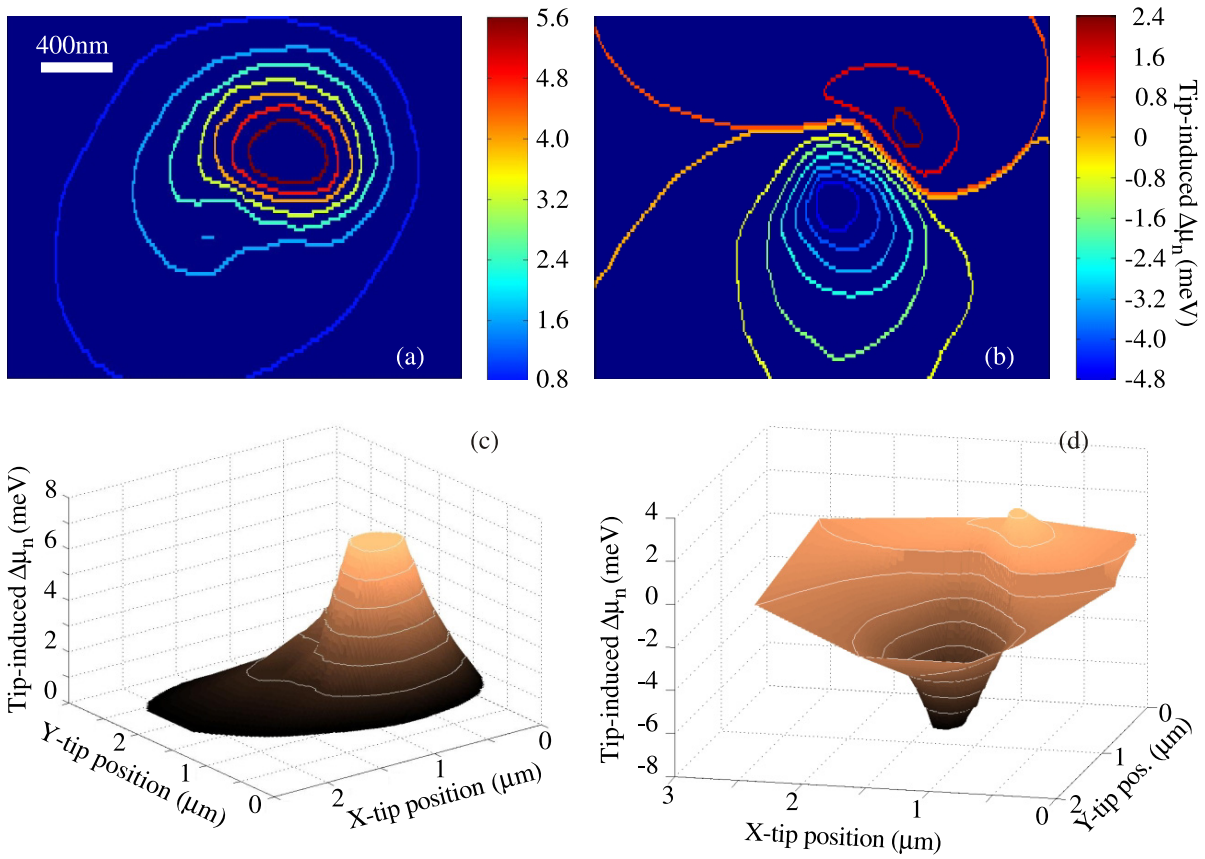

Figure 3. Reconstruction of the tip–dot interaction potential $\Delta\mu_n$ obtained from scanning-gate images for two different U_{tip}. Pictures (a) and (b) show contour lines representing constant tip–dot interaction potential (lines along current resonances). They were obtained from figure 2(a) ($U_{\mathrm{tip}} = 0\,\mathrm{mV}$) and figure 2(f) ($U_{\mathrm{tip}} = 510\,\mathrm{mV}$). The energetic separation of the contour lines is taken to be the average charging energy of the dot. (c) Three-dimensional image of $\Delta\mu_n$ reconstructed from (a) for $U_{\mathrm{tip}} = 0\,\mathrm{mV}$. The interaction potential is repulsive. (d) Three-dimensional image of $\Delta\mu_n$ reconstructed for $U_{\mathrm{tip}} = 510\,\mathrm{mV}$. The interaction potential is mainly attractive.

The finding that the two tips were more than 600 nm displaced from each other, the very different contact potential differences of the two and the fact that both offered a comparable resolution in scanning-gate images allowed us to use each of them separately for further investigations of the QD, if the scan range was kept well below their separation. Such measurements will be described in section 3.4.

We continue with a discussion of the width and separation of conductance peaks in the scanning-gate images of figure 2. It can be seen, e.g., in figure 2(a) that the outer ring-shaped conductance resonances appear to be broader than the inner ones. At the same time, the spacing between the outer resonances is significantly larger than that of the inner ones. Both effects are manifestations of the exact spatial shape of the tip–dot interaction potential. Energy differences ΔE, like the energetic spacing of conductance peaks, or the width of conductance peaks

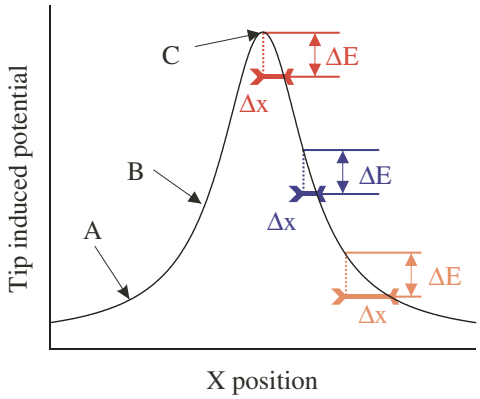

Figure 4. Schematic drawing illustrating the influence of a repulsive tip–dot interaction on the width and spacing of tip-induced conductance resonances. The tip-induced change of μ_n is sketched in one dimension as a Lorentzian curve. ΔE represents the thermal broadening/spacing of conductance peaks. Δx is the distance necessary to go either through one Coulomb peak or from one Coulomb peak to the next one.

(about $3.5\,kT$ for thermal broadening) are, to lowest order, translated into spatial separations $|\Delta\vec{r}|$ by

$$|\Delta\vec{r}| = \frac{\Delta E}{|\nabla\mu_n(\vec{r})|}. \tag{3}$$

If the spatial gradient of the tip–dot interaction $|\nabla\mu_n(\vec{r})|$ is small, conductance peaks are far apart in space and their spatial width is large as well. The opposite is true for large $|\nabla\mu_n(\vec{r})|$. Figure 4 illustrates this situation in one dimension with a Lorentzian-shaped model curve for $\mu_n(x)$. Large spacings and widths of conductance peaks are expected for large lateral tip–dot separations (A) and for the case that the tip sits directly above the dot (C). The latter situation in which $|\nabla\mu_n(\vec{r})|$ can become zero will be further discussed in section 3.4. Small separations and widths of conductance resonances are observed in the intermediate regime of tip–dot separation (B), where the slope of $|\nabla\mu_n(\vec{r})|$ is largest. The typical gradient of the tip–dot interaction potential observed in our experiments is $|\nabla\mu_n(\vec{r})| = 2$–$4\,\mu\text{eV nm}^{-1}$.

We conclude the analysis of the scans in figure 2 with a discussion about the dependence of the conductance peak amplitude $G_{\max}$ on tip position. In figures 2(a)–(e), it becomes evident that the amplitude for each of the conductance fringes in 'set B' is enhanced with the tip to the right of the fringe centre, while it is strongly suppressed with the tip to the left. The conductance peak amplitude $G_{\max}$ obtained from conductance fringes of 'set T' in figure 2(f) shows the opposite behaviour, i.e., peaks are enhanced to the left of the centre of the fringes and weaker to the right. For both sets, the action of the tip is much stronger on the left of the QD (i.e., the respective fringe centre) indicating that the coupling to the left lead dominates $G_{\max}$. This behaviour of the two sets of fringes is another manifestation of the double-tip with a repulsive tip and an attractive twin.

3.4. Scanning-gate measurements in the QD interior

A second series of scans concentrated on a small scan range of 300×300 nm covering the expected electronic size of the dot with the twin-tip that lead to the 'set T' of fringes in figure 2. The position of the images relative to the structure is shown in figure 5(j). The set of figures 5(a)–(i) is a selection of scanning-gate images from a series taken for tip-voltages between 260 mV and 85 mV in steps of 5 mV. The tip was scanned at a constant distance of 150 nm from the surface. The pixel separation in the images is 3.37 nm, i.e., small compared to the estimated electronic Fermi wavelength of about 30 nm. Compared to the series of images in figure 2 the gate-voltage parameters for the dot were optimized for these measurements such that the coupling of the dot to the leads was better balanced.

Figure 5(a) taken for $U_{\mathrm{tip}} = 190$ mV shows one complete ring-shaped conductance resonance and a fully developed CB valley in its centre. The ring size is about 250 nm $\times$ 200 nm, i.e., about the estimated electronic size of the QD. Decreasing U_{tip} to 180 mV in figure 5(b) shrinks the size of the conductance resonance ring and weakens the blockade in its centre. At $U_{\mathrm{tip}} = 175$ mV (figure 5(c)), the conductance resonance is further shrunk and only a small decrease of the conductance in its centre is reminiscent of the CB. Eventually, in figure 5(d) ($U_{\mathrm{tip}} = 170$ mV), the conductance resonance ring has turned into a spot of enhanced conductance and the blockade in its centre has completely disappeared. In figures 5(e) and (f) ($U_{\mathrm{tip}} = 160$ and 155 mV), the spot shrinks continuously and the measured peak current gets smaller as well. The size of the spot in figure 5(f) is much smaller than the electronic dot size and it disappears completely in figure 5(g) ($U_{\mathrm{tip}} = 135$ mV). In the latter image, a new resonance ring has appeared that starts the same cycle as described in figure 5(h). In figures 5(h) and (i), the tip is less invasive with $U_{\mathrm{tip}} = 110$ and 100 mV, respectively. As a consequence, the conductance resonances appear to be more extended in space as compared to the previous images. Figure 5(i) shows a sudden decrease of conductance marked as (r). This decrease was seen in several images and is probably due to a parametric charge rearrangement in the sample close to the QD. However, there is no sign of any further significant substructure within the central spots of resonant conductance.

By lowering U_{tip} even further, the repulsive potential of the other tip became dominant in the selected scan range inhibiting a truly non-invasive scan. In the cycle of disappearing resonances, figure 5(h) corresponds to figures 5(b) and (i) as well as to figure 5(d). The resonant features in these figures 5(h) and (i) are shifted a few tens of nanometres as compared to figures 5(b) and (d) due to the increasing influence of the other tip.

3.5. Discussion in terms of the model

The data described above can be discussed in terms of the model represented by equations (1) and (2). However, unlike in the discussion of figure 2 where the finite gradient of $\mu_n(\vec{r})$ played an important role due to large or intermediate tip–dot separations, we are now interested in the behaviour of $\mu_n(\vec{r})$ when the tip is scanning directly above the QD. In this case, various scenarios can arise depending on the tip-surface separation, the tip radius, the tip bias and the depth of the 2DEG below the surface. In our context, it is of interest to decide whether the experimental setting is suitable for probing the QD interior locally.

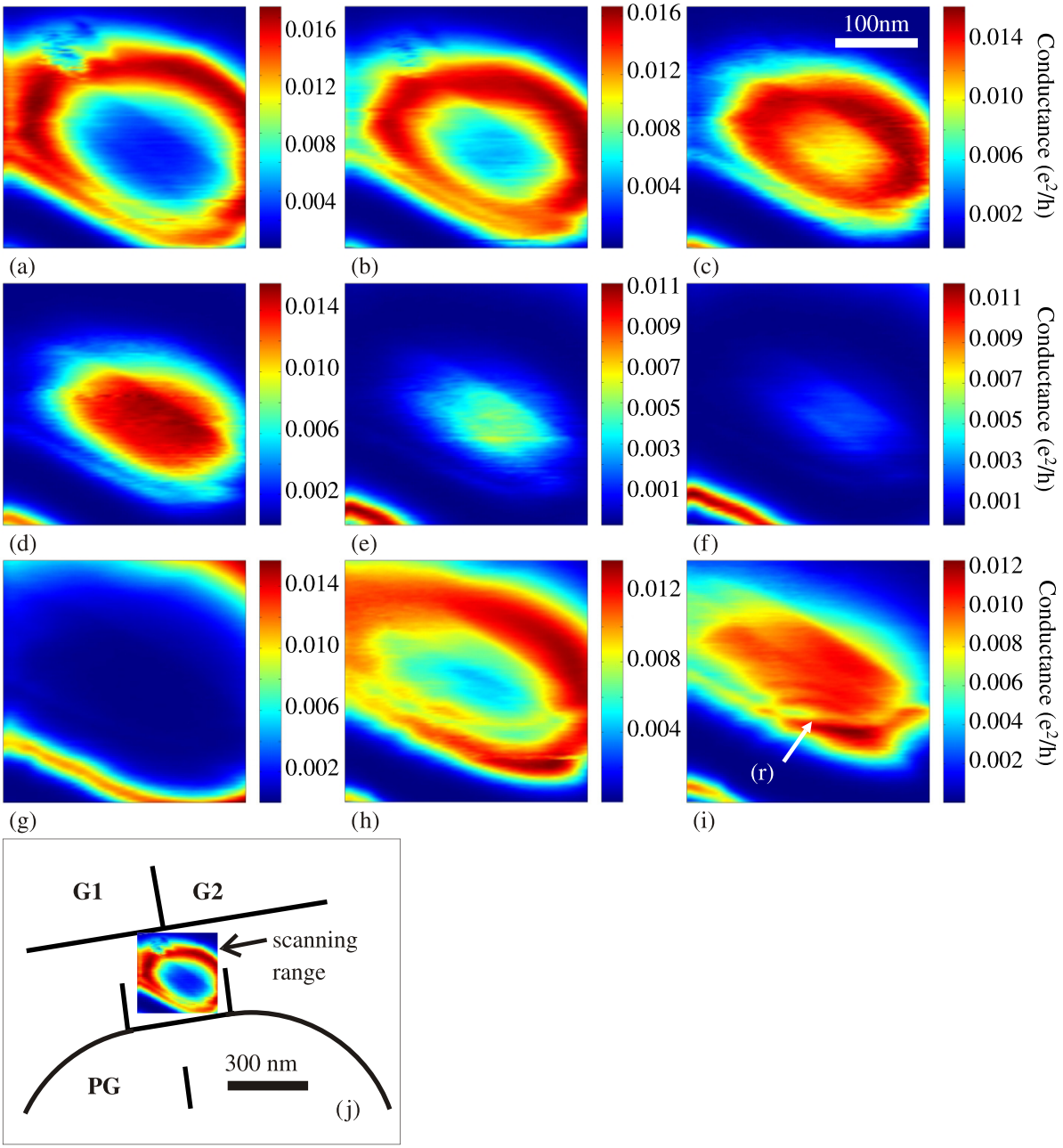

Figure 5. Scanning-gate images (300 × 300 nm) showing the development of ring-shaped conductance resonances in the central dot region when U_{tip} is varied. The attractive tip of the double-tip was situated above the dot for these images. The conductance resonance rings shrink continuously when U_{tip} is decreased. The tip-voltages are (a) $U_{\mathrm{tip}} = 190$ mV, (b) 180 mV, (c) 175 mV, (d) 170 mV, (e) 160 mV, (f) 155 mV, (g) 135 mV, (h) 110 mV, (i) 100 mV, and (j) position of the scans with respect to the dot.

Considering the tip–surface separation of 150 nm for the images in figure 5 and an electronic size of the dot only about a factor of 2 larger, we cannot expect to resolve much details in the dot interior even with an arbitrarily sharp tip. However, it turns out that the resolution is just sufficient to establish an analysis method and get a first glimpse of details within the QD.

For this analysis, we solve equation (2) for $\mu_n(\vec{r})$ in order to determine it (up to a constant) directly from the measured conductance image $G(x, y)$, provided that we concentrate on a single conductance resonance n. We obtain

$$\mu_n(\vec{r}) = \pm 2kT \operatorname{arcosh}\left(\sqrt{\frac{G_{\max}(\vec{r})}{G(\vec{r})}}\right), \tag{4}$$

where $\mu_n(\vec{r})$ is measured relative to the electrochemical potential in the source and drain. Care has to be taken when inverting the cosh-function because its inverse has two branches, in our case accounted for by the sign ambiguity. We determine a reasonable approximation for $G_{\max}(\vec{r})$ from an image, where the ring-shaped conductance resonance is fully developed (e.g., figure 5(h)). Three points are chosen around the ring on the maximum of the conductance for defining a plane that serves as a first-order approximation for $G_{\max}(\vec{r})$.

The results of the analysis described by equation (4) are shown in figure 6. Figure 6(a) is raw data from the series of scans shown in figure 5, taken at $U_{\text{tip}} = 100$ mV. In figures 6(b) and (c), we show the results of the analysis plotted along the lines labelled (b) and (c) in figure 6(a). The four curves correspond to tip-voltages changing from $U_{\text{tip}} = 100$ to 85 mV in steps of 5 mV. The offset between these curves reflects the change in tip-voltage.

The four curves in figure 6(b) show very similar behaviour. As the tip is traversing the dot, its chemical potential initially decreases, stays at an almost constant value and then rises again when the tip moves away from the dot. This observation is the evidence for the tip probing the dot interior rather than the dot probing the tip. The appearance of the plateau in $\mu_n(\vec{r})$ in the centre of the dot demonstrates that the tip-induced potential in the plane of the dot is smaller than the electronic width of the QD along this line by the width of the plateau which is about 80 nm.

The four curves in figure 6(c) show a similar behaviour, the plateau is most pronounced for the lowest two tip-voltages. The width of the plateau of up to 160 nm is consistent with the fact that the dot is more extended in this direction (cf figure 5(j)). The finite extent of the tip along the two chosen directions enters $\mu_n(\vec{r})$ beyond the plateau region where it steadily increases. If the shape of the tip is anisotropic in these two directions the map of $\mu_n(\vec{r})$ will be distorted correspondingly.

In the case of figure 6(b), all the curves can be shifted to fall on to a single curve. Within the model of equation (1) this means that the electrostatic lever arm of the tip varies very little along the line of analysis. In fact, it can be quantitatively determined from the separation of two neighbouring curves to be $\alpha_{\text{tip}} = 0.012$, in agreement with the value determined from CB diamond measurements presented in table 1 for the tip in position 1 indicated in figure 7. The small reproducible features appearing on the plateau may be the signature of the influence of the tip on the actual quantum states in the dot, i.e., a glimpse of the quantum structure within the QD.

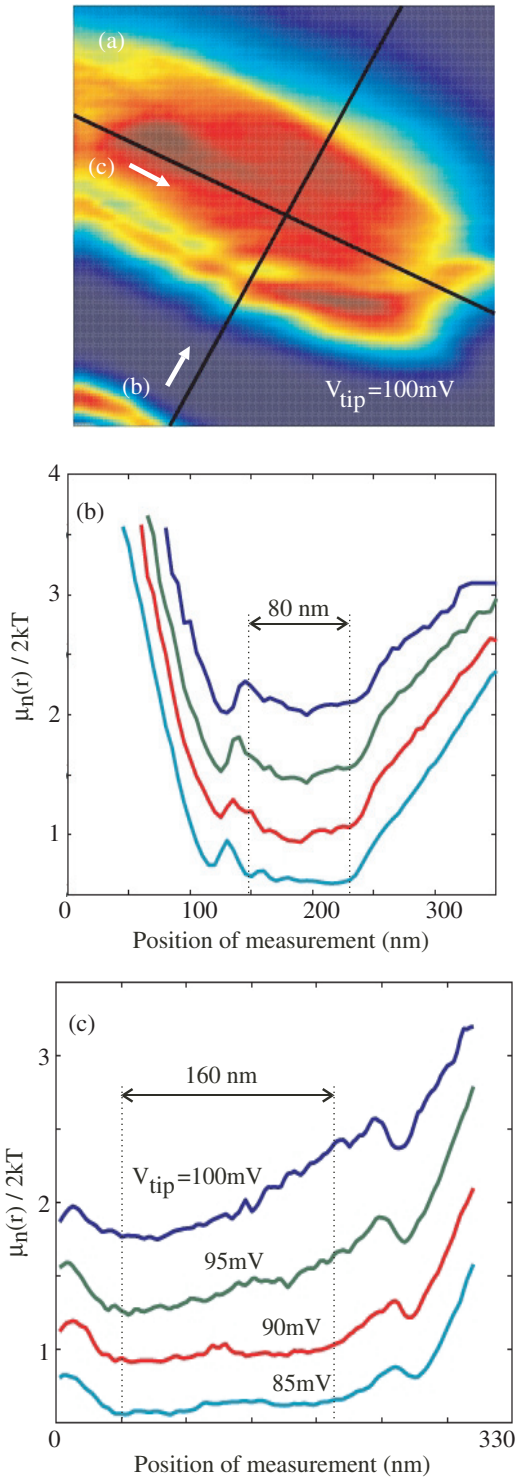

Figure 6. Analysis of the development of μ_n for various U_{tip}. μ_n was calculated using equation (4). (a) Map of μ_n for the image in figure 5(i) with a scan area of 300 nm × 300 nm. The two lines (marked as (b) and (c)) indicate along which lines the data were analysed. (b) Development of μ_n along line (b) for $U_{\text{tip}} = 85, 90, 95$ and 100 mV. (c) Development of μ_n along line (c) for the same values of U_{tip} as in the previous case.

Table 1. Influence of the tip position relative to the dot on the lever arms of gates and tip and on the charging energy e^2/C_Σ The absolute lever arms of the PG and the charging energy e^2/C_Σ were determined directly from CB diamonds. The absolute lever arms of all other gates were calculated using measured relative lever arms.

	Absolute lever arm				
Pos.	PG	Tip	G1	G2	e^2/C_Σ (μeV)
1	0.129 ($\pm$0.01)	0.013 ($\pm 7 \times 10^{-4}$)	0.107 ($\pm$0.008)	0.065 ($\pm$0.005)	733 ($\pm$49)
2	0.114 ($\pm$0.017)	0.0014 ($\pm 6 \times 10^{-4}$)	0.093 ($\pm$0.008)	0.054 ($\pm$0.008)	772 ($\pm$10)
3	0.138 ($\pm$0.011)	0.0017 ($\pm 4 \times 10^{-4}$)	0.111 ($\pm$0.009)	0.069 ($\pm$0.007)	808 ($\pm$8)
4	0.119 ($\pm$0.008)	0.0018 ($\pm 1 \times 10^{-4}$)	0.101 ($\pm$0.006)	0.058 ($\pm$0.004)	786 ($\pm$12)
5	0.132	0.004	0.111	0.0654	732 ($\pm$34)
6	0.133	0.005	0.111	0.0653	810 ($\pm$10)
7	0.096 ($\pm$0.016)	0.009 ($\pm$0.001)	0.082 ($\pm$0.014)	0.044 ($\pm$0.008)	766 ($\pm$42)

From the above analysis it becomes clear why conductance resonance features can be observed in scanning-gate images that are much smaller than the electronic size of the QD. This is even the case, if the tip radius is larger than in our experiment and no plateau is observed in $\mu_n(\vec{r})$. It can be easily shown from equation (2), if a parabolic approximation is made for $\mu_n(\vec{r})$ around the dot centre. The size of conductance resonance rings depends in this situation on the curvature of $\mu_n(\vec{r})$ where it is maximal. Sufficiently large curvature can lead to rings smaller than the electronic size of the dot even though the full-width at half-maximum of the tip–dot interaction potential may be significantly larger. Tip-voltages closer to the contact potential difference lead to a smaller curvature and therefore to a larger size of comparable conductance resonances.

4. Effects of the tip on lever arms and charging energy

As mentioned in the discussion of equation (1), it is expected that the presence of the tip close to the QD may change the lever arms of the gates and the charging energy of the dot. We investigated this influence by placing the tip at several representative x–y-positions at a distance of 200 nm from the surface as indicated in figure 7. In each position CB diamonds were measured and the relative lever arms of the gates were determined. The results are summarized in table 1. As expected, the lever arm of the tip is a strong function of its position relative to the QD. The lever arms of the gates PG, 'G1' and 'G2' were also found to change significantly for the tip in different positions giving evidence for the screening effects discussed in connection with equation (1). The relatively unsystematic change of the lever arms with tip position is a consequence of the rather peculiar shape and double-tip character of this particular sensor. For a cylindrically symmetric sensor, a rather symmetric and systematic dependence of the lever arms on tip position would be expected. The same argument applies to the corresponding charging energies given in the last column of table 1. The values also vary significantly from position to position although a more symmetric and systematic dependence would be expected for a single symmetric tip.

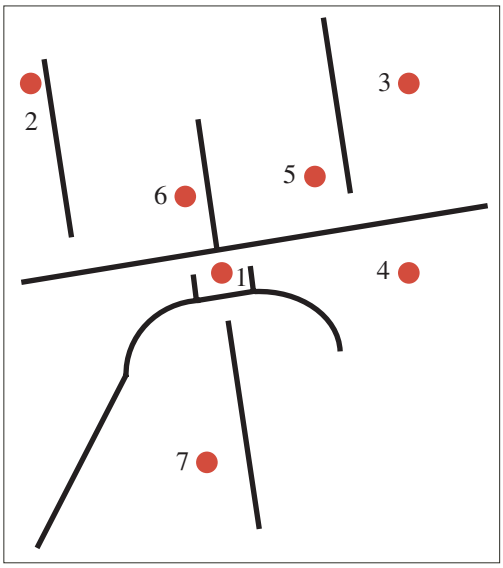

Figure 7. Positions of the tip during the measurements of the tip-position dependence of the lever arms.

5. What are the conditions for true wave function mapping?

From the above analysis it becomes clear that certain criteria need to be fulfilled for wave function mapping in a lateral semiconductor QD. Firstly, the QD has to be operated in the single-level transport regime in which a single wave function dominates the conductance resonance. This requires an electron temperature well below that determined in the presented experiments and dot sizes. In addition, a lithographically smaller dot would help for achieving the single-level transport regime by increasing the single-particle level spacing Δ. The second requirement for wave function mapping is a tip-diameter small compared to the Fermi wavelength which is of the order of 30–50 nm. Such tip-diameters were actually realized with our electrochemically sharpened tips as confirmed by scanning electron microscopy. Thirdly, the separation between the tip and the 2DEG needs to be smaller than the Fermi wavelength, i.e., shallow 2DEGs are required with cap layers of thickness less than 50 nm. This requirement is met in our samples. The tip–surface separation has to be minimized, but is less crucial than the cap layer thickness due to the high relative dielectric constant of the Ga[Al]As material.

Wave function mapping experiments would have to be performed at voltages where the tip–dot interaction is very close to the least invasive situation in order to perturb the QD wave functions only slightly. Highest sensitivity can be expected in the tail of a conductance peak at an operating point in PG where the slope of the conductance is maximized.

6. Conclusions

The presented scanning-gate experiment demonstrates the progress made and the problems encountered in the local investigation of quantum states in semiconductor QDs. Many crucial requirements such as reliable operation of the scanning probe microscope at cryogenic

temperatures, coarse positioning of the sample and the long-term stability of the sample during scanning have been met. The spatial resolution has been put to its limits, so far given by the quality of the tip, the cleanliness of the sample surface and the accessible electron temperature. Within these limits, the expected optimum in resolution has been demonstrated, allowing scanning-gate images within the electronic area of the QD. The results of these experiments promise the feasibility of accessing the local quantum mechanical probability distributions of electronic states in QD structures and even more complicated coupled mesoscopic systems. Such a technique has the potential to improve our abilities to design and tailor quantum states for highly demanding applications such as quantum communication and quantum information processing.

Acknowledgments

We thank T Vančura for his contribution to the experimental setup. Financial support from the Swiss Science Foundation (Schweizerischer Nationalfonds) via NCCR Nanoscience is gratefully acknowledged.

References

[1] Nielsn M A and Chuang I L 2000 *Quantum Computation and Quantum Information* (Cambridge: Cambridge University Press)
[2] Quantum Information Science and Technology Roadmap, available at http://qist.lanl.gov/
[3] Kouwenhoven L P, Schön G and Sohn L L 1997 *NATO ASI Conf. Proc.* (Dordrecht: Kluwer) pp 105–214
[4] Grabert H and Devoret M H (eds) 1991 *Single Charge Tunneling* (New York: Plenum)
[5] Fuhrer A, Lüscher S, Ihn T, Heinzel T, Ensslin K, Wegscheider W and Bichler M 2001 *Nature* **413** 822
[6] Lindemann S, Ihn T, Heinzel T, Zwerger W, Ensslin K, Maranowski K and Gossard A C 2002 *Phys. Rev.* B **66** 195314
[7] Kyriakidis J, Pioro-Ladriere M, Ciorga M, Sachrajda A S and Hawrylak P 2002 *Phys. Rev.* B **66** 35320
[8] Hanson R, Witkamp B, Vandersypen L M, Willems van Beveren L H, Elzerman J M and Kouwenhoven L P 2003 *Phys. Rev. Lett.* **91** 196802
[9] Fuhrer A, Ihn T, Ensslin K, Wegscheider W and Bichler M 2003 *Phys. Rev. Lett.* **91** 206802
[10] Loss D and DiVincenzo D P 1998 *Phys. Rev.* A **57** 120
[11] Burkhard G, Engel H-A and Loss D 2000 *Fortschr. Phys.* **48** 965
[12] Ciorga M, Sachrajda A S, Hawrylak P, Gould C, Zawadzki P, Jullian S, Feng Y and Wasilewski Z 2000 *Phys. Rev.* B **61** R16315
[13] Kouwenhoven L P, Austing D G and Tarucha S 2001 *Rep. Prog. Phys.* **64** 701
[14] Hanson R, Witkamp B, Vandersypen L M K, Willems van Beveren L H, Elzerman J M and Kouwenhoven L P 2003 *Phys. Rev. Lett.* **91** 196802
[15] Zumbühl D M, Marcus C M, Hanson M P and Gossard A C 2004 *Phys. Rev. Lett.* **93** 256801
[16] Yoo M J, Fulton T A, Hess H F, Willett R L, Dunkleberger L N, Chichester R J, Pfeiffer L N and West K W 1997 *Science* **276** 579
[17] Ilani S, Martin J, Teitelbaum E, Smet J H, Mahalu D, Umansky V and Yacoby A 2004 *Nature* **427** 328
[18] Finkelstein G, Glicofridis P I, Ashoori R C and Shayegan M 2000 *Science* **289** 90
[19] Topinka M A, LeRoy B J, Westervelt R M, Shaw S E J, Fleischmann R, Heller E J, Maranowski K D and Gossard A C 2001 *Nature* **410** 183
[20] Crook R, Smith C G, Graham A C, Farrer I, Beere H E and Ritchie D A 2003 *Phys. Rev. Lett.* **91** 246803
[21] Woodside M T and McEuen P L 2002 *Science* **296** 1098
[22] Pioda A, Kicin S, Ihn T, Sigrist M, Fuhrer A, Ensslin K, Weichselbaum A, Ulloa S E, Reinwald M and Wegscheider W 2004 *Phys. Rev. Lett.* **93** 216801

[23] Fallahi P, Bleszynski A C, Westervelt R M, Huang J, Walls J D, Heller E J, Hanson M and Gossard A C 2005 *Nano. Lett.* **5** 223
[24] Mendoza M and Schulz P A 2003 *Phys. Rev.* B **68** 205302
[25] Held R, Vancura T, Heinzel T, Ensslin K, Holland M and Wegscheider W 1998 *Appl. Phys. Lett.* **73** 262
[26] Heinzel T, Held R, Lüscher S, Ensslin K, Wegscheider W and Bichler M 2001 *Physica* E **9** 84
[27] Fuhrer A, Dorn A, Lüscher S, Heinzel T, Ensslin K, Wegscheider W and Bichler M 2002 *Superlatt. Microstruct.* **31** 19
[28] Ihn T 2004 *Electronic Transport in Mesoscopic Semiconductor Structures* (*Springer Tracts in Modern Physics* vol 192) (New York: Springer)
[29] Beenakker C W J 1991 *Phys. Rev.* B **44** 1646
[30] Vancura T, Kicin S, Ihn T, Ensslin K, Bichler M and Wegscheider W 2003 *Appl. Phys. Lett.* **83** 2602